Cognitive Radar Network: Cooperative Adaptive Beamsteering for Integrated Search-and-Track Application

RIC A. ROMERO, Senior Member, IEEE
Naval Postgraduate School

NATHAN A. GOODMAN, Senior Member, IEEE
University of Oklahoma

Cognitive radar (CR) is a paradigm shift from a traditional radar system in that previous knowledge and current measurements obtained from the radar channel are used to form a probabilistic understanding of its environment. Moreover, CR incorporates this probabilistic knowledge into its task priorities to form illumination and probing strategies, thereby rendering it a closed-loop system. Depending on the hardware's capabilities and limitations, there are various degrees of freedom that a CR may utilize. Here we concentrate on spatial illumination as a resource, where adaptive beamsteering is used for search-and-track functions. We propose a multiplatform cognitive radar network (CRN) for integrated search-and-track application. Specifically, two radars cooperate in forming a dynamic spatial illumination strategy, where beamsteering is matched to the channel uncertainty to perform the search function. Once a target is detected and a track is initiated, track information is integrated into the beamsteering strategy as part of CR's task prioritization.

Manuscript received July 20, 2011; revised March 9, 2012; released for publication July 12, 2012.

IEEE Log No. T-AES/49/2/944509.

Refereeing of this contribution was handled by R. Narayanan.

Authors' addresses: R. Romero, Naval Postgraduate School, Department of Electrical and Computer Engineering, 833 Dyer Rd., Sp-Hall Rm 544A, Monterey, CA 93943, E-mail: (rnromero@nps.edu); N. Goodman, School of Electrical and Computer Engineering, University of Oklahoma, Norman, OK.

I. INTRODUCTION

One of the earlier authors to explore the subject of intelligent radar is Fuhrmann [1, 2], where he termed such a smart radar platform as an active-surveillance system. A more recent work that utilizes the knowledge-aided adaptive approach to radar systems is [3]. In [4] Haykin formalized the notion of cognitive radar (CR) to be a technological solution for performance optimization in resource-constrained and interference-limited environments. From this statement it is clear that for a radar system to be cognitive, it must operate such that it mitigates and, if possible, exploits various interference sources that it is faced with. In doing so it must use its resource efficiently, whether this resource is energy, time, or otherwise. For example, in surveillance applications where a search function may be the main objective of a system or mission, then detection of targets is the ultimate goal. Usually, the surveillance area is very large as compared with the beamwidth of the sensor or antenna array. As such, in traditional systems, a uniform or rasterized search pattern is used in illuminating the scene. But in a large area, various portions may have different likelihoods of targets being present/absent. In other words various areas have more certainty or uncertainty than others. As such, a cognitive system performing detection of targets should place more illuminations to areas of most uncertainty.

The advent of CR is still in its early stages, and CR applications are being investigated. In terms of system identification/target recognition, various contributions have been made. Addressing this notion of a closed-loop intelligent radar, one early work was presented in [5], where a CR platform was used for target recognition. This CR utilized the waveforms designed in [6], [7]. These waveforms were modified as adaptive transmit waveforms for discrimination of known targets. It was shown that this CR framework could reduce the energy required for identification. In [8], [9] this closed-loop radar strategy was applied to discrimination of target classes rather than a finite ensemble of known targets. In [10] a new, multi-band CR performing target recognition was demonstrated. In [11] an ultrawideband cognitive interrogator network was introduced. In [12] a CR platform was used for search-and-track applications. The cells of the surveillance area were assigned initial probabilities, which were updated as more measurements were collected. The current probability map can be termed as the probabilistic understanding of the channel. While the main contribution of this paper is the introduction of a cognitive radar network (CRN) for integrated search-and-track applications, the contributions are multiple-fold in nature. We develop a system of two radars that performs a cooperative search of a surveillance area by networking the two

radars, where each radar is able to measure two position parameters and one velocity parameter. By a unique fusion of measurements via probabilistic methods, the two radars form a four-dimensional map of the radar channel. Each resolution cell in this four-dimensional matrix carries a probability of a target being present. Via the probability update methodology presented here, the two radars are able to update these probabilities by the most recent radar measurement. Moreover, the updated probabilities are incorporated in forming the radar's beamsteering strategy to efficiently search for targets. This feedback mechanism is basic to cognitive systems. As such, we form the beginnings of a CRN. Moreover, we configure the CRN to track detected targets. Here, we form an adaptive beamsteering strategy for an integrated search-and-track such that a balance between the search priority and preserving track quality is accommodated. The delicate act of balancing priorities is also a cognitive signature.

From the discussion of a surveillance area having cells of target presence probabilities, it is clear that a measure of uncertainty is needed. From information theory entropy is a natural measure of uncertainty. This metric is exploited and proves useful in efficient utilization of resources for this CR application. That is, the CR performs the search surveillance with the beamsteering strategy dynamically tailored to the area's likelihood of target presence/absense. With this beamsteering strategy it is said that the spatial illumination is matched to the area's uncertainty. Indeed, the idea of designing resource strategies "matched" to uncertainties of interest is critical in CR technology, such that it ensures that the CR resources are applied efficiently [5, 10]. In traditional radar no provision is applied to "adaptively" change the beamsteering pattern while in operation. In contrast CR is a transmitter-centric closed-loop radar system, where the transmit beamsteering strategy is dynamically formed, i.e., it must be designed real-time in an effort to respond, mitigate, and even exploit its environment. Consequently, received measurements are used to update the current probabilistic understanding of the channel. Then, CR may use this understanding to pinpoint the location where the next illumination beam should be placed [12]. This idea was extended to form a CRN in a preliminary work reported in [13]. It is evident that efficient utilization of the spatial dimension as a resource for CR is performed by matching the illumination pattern to the radar channel environment. Specifically, in this application, the CRN developed in this paper is a two-platform radar system designed to perform surveillance of moving targets. In this work the two radar platforms are static. The two radars cooperate in searching for moving targets and in forming a four-parameter track once target detection is declared. Search and track functions present two competing priorities to the CRN in its use of beamsteering strategy as a resource from each radar. The CRN developed in this work is designed such that search and track priorities are accommodated. In other words both functions are well integrated in the closed-loop nature of the CR system. The individual radars considered here are capable of measuring three parameters (e.g. range, Doppler, and angle). The CRN, which maintains a four-parameter track, forms a four-dimensional probabilistic understanding of the channel. Specifically, the probabilistic understanding is a 4-D matrix or ensemble of cell probabilities of target presence. Each radar is blind to the parameter or dimension that it cannot measure. For a single radar the cells in the dimension in which it is blind to are said to be "ambiguous" (but not in the traditional sense of the ambiguity function [14]). Thus, probability update methods are needed for radar receiving measurements with ambiguous cells. Section II presents in detail the system we design to be a CRN, defines a cell in the context of the system being considered, and presents an update procedure needed to update probabilities which can be applied to the ambiguous cells. Multiple hypotheses testing (MHT) and Bayes' rule are the engines on which the procedure is based. Section III is where we begin to develop our CRN, and it discusses aspects of radar systems that are of importance. Section IV discusses two beamsteering strategies for the two radar platforms: traditional and search-only adaptive. Section V discusses the integrated search-and-track adaptive beamsteering strategy. In Section VI we summarize the concepts needed to form a CRN and illustrate, via a block diagram, the closed-loop nature of the two-platform system that performs integrated search-and-track functions, where a compromise between the two priorities is accommodated. Sections VI-A and VI-B present various search-and-track simulation examples. Finally, in Section VI-C, a detection performance comparison is made between a CRN and a two-platform radar system employing traditional rasterized search pattern via Monte Carlo simulations. Section VII contains our conclusions.

II. SYSTEM DESCRIPTION, PROBABILISTIC REPRESENTATION, AND PROBABILITY UPDATE

A. System Desription

Our interest is a radar system that performs integrated search-and-track. Instead of one radar platform, we are interested in two radar platforms that illuminate the same surveillance area. Figure 1 shows an overall picture of the system that we are trying to build. The two radars search for moving targets in a surveillance area and establish four-parameter tracks (two positions and two velocities as shown in the figure). It is our goal for the two radar platforms to

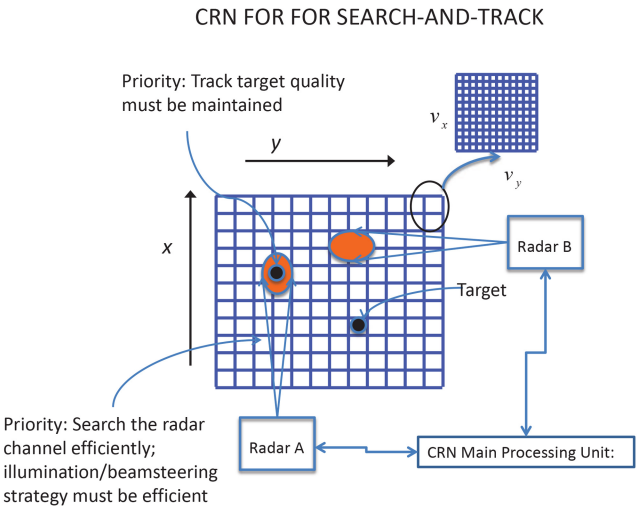

Fig. 1. Overall picture of CRN for search-and-track application.

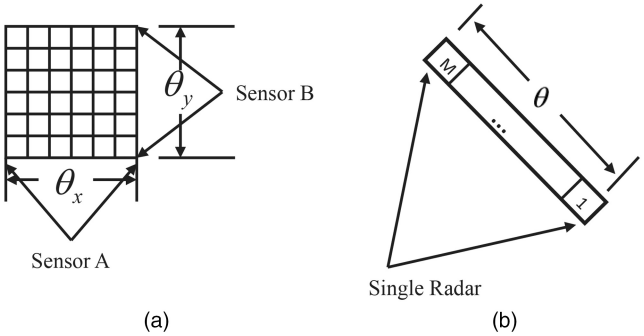

Fig. 2. (a) Two sensors forming the probability map: Parameter θ_y is ambiguous to sensor A and parameter θ_x is ambiguous to sensor B. (b) Single radar updating a 1-D probability ensemble.

cooperate in searching for moving targets and forming tracks for the detected targets. Specifically, it is our goal for the two radars to cooperate in forming a dynamic spatial beamsteering strategy that responds to two competing priorities: 1) the continual search for targets and 2) the maintenance of target tracks. As shown in Fig. 1, we are interested in a four-parameter target space. In our scenario each radar is able to measure three parameters: 2 position parameters and one velocity parameter. Due to the geometry of the problem, only one velocity parameter can be measured by each radar. Each cell in that 3-D space captures the cubic (two position and one velocity) resolution of each radar as dictated by their waveforms. It is our goal that these radars form a network such that a complete 4-D parameter description of the channel can be formed. The radars are configured such that the position resolutions are the same so that a fusion resulting in a 4-D matrix that consists of target resolution cells can be completed. Each resolution cell in the 4-D parameter map will have a probability of a target being present. Thus, the probabilistic understanding or representation of the radar channel being considered is a 4-D probability map.

B. Probability Update Methodology

Probability update methodologies needed for the formation of a CRN were reported in our preliminary work [15]. Here, we present the main engine of the update methodology discussed in [15]. Consider two sensors shown in Fig. 2(a). Sensor A can measure a parameter θ_x but not θ_y, and vice versa for sensor B. In Fig. 2(a) the channel may be described by a 2-D map, where each cell is described by its (θ_x,θ_y) coordinate. In practice one may think of these parameters as velocities, which are measured by Doppler frequencies. When the motion is orthogonal to the radar line-of-sight, then the tangential velocities for these cells cannot be measured, which results in ambiguity. The job of the probability update methodology is to update probabilities for these cells. We use a 2-D example to illustrate how probabilities are calculated in a simpler example and note that the methodology can easily be extended to our multidimensional problem in Fig. 1. Since there are M θ_x cells and M θ_y cells, there are a total of M^2 cells. For sensor A note that under each θ_x-cell, there are M θ_y cells that are ambiguous in the sense that sensor A cannot resolve them. Similarly, for sensor B, under each θ_y-cell, there are M cells that are ambiguous. Hence, in this simplified example, the probabilistic description of the channel is a list of M^2 probabilities. The goal of the update procedure is to update these cell probabilities as new data are received.

We assume the presence of a target in one cell to be independent of the presence of targets in other cells. We assume a target to be physically smaller than a cell's physical extent and, therefore, cannot occupy multiple cells, such that the cells may not be correlated. Therefore, there are 2^M possible permutations of the overall target environment, where a permutation is a unique combination of target presence across the resolution cells and a permutation is itself characterized by a probability of being true. This two-platform cooperative system needs a way to update the probability ensemble after each radar illuminates the channel. First, we address how a single sensor measuring a parameter θ with M cells, as shown in Fig. 2(b), would update its cell probabilities with received measurements. Then, the approach is easily extended to the two-sensor case, where the sensors cooperate to update a 2-D probability matrix [15].

Let the 1-D vector of initial cell probabilities be given by

$$\mathbf{P}_0 = [P_{M,0} \ldots P_{m,0} \ldots P_{2,0} \quad P_{1,0}]$$

where $P_{m,0}$ is the initial prior for the mth cell. Consider a sensor that produces an N-element measurement vector with each data collection. Let $\mathbf{s}_m$ be the signal produced at the sensor if a target is present in the mth resolution cell, and let the measurement indices

be denoted by $n = 0, 1, \ldots, N-1$. For a radar system a target parameter is estimated via a frequency measurement (e.g., Doppler for velocity parameter), so we let the frequency produced by the presence of a target in the mth cell be denoted by f_m. When these cell frequencies are the same, the cells are ambiguous. When the frequencies differ, it may be possible to resolve the cells. The signal produced by a target in the mth cell is proportional to a normalized steering vector given by

$$\mathbf{s}_m = \frac{1}{\sqrt{N}} \exp(j2\pi f_m [0 \cdots n \cdots N-1]^T). \tag{1}$$

It is necessary to assume a signal model for the measurements. For convenience let the targets be deterministic, i.e., known amplitude and phase, and let the noise be additive white Gaussian. Other scenarios may produce measurements with different probability density functions (pdfs), but the probability update procedure is applicable to these cases (assuming the pdfs are known). The environment can be described by a multiple hypotheses framework. The hypotheses in this framework are given by

$$\begin{aligned} &H_0 : \mathbf{z} = \mathbf{n} \\ &H_1 : \mathbf{z} = \mathbf{s}_1 + \mathbf{n} \\ &H_2 : \mathbf{z} = \mathbf{s}_2 + \mathbf{n} \\ &H_3 : \mathbf{z} = \mathbf{s}_1 + \mathbf{s}_2 + \mathbf{n} \\ &H_4 : \mathbf{z} = \mathbf{s}_3 + \mathbf{n} \\ &\vdots \\ &H_{2^M-1} : \mathbf{z} = \mathbf{s}_1 + \mathbf{s}_2 + \cdots + \mathbf{s}_M + \mathbf{n}. \end{aligned} \tag{2}$$

Each hypothesis H_i is a "joint" hypothesis corresponding to a unique permutation of target presence/absence in the individual cells. For notational convenience we convert the joint hypothesis subscript i to its binary representation of $i = 0\cdots00, 0\cdots01, 0\cdots10, 0\cdots11, \ldots, 1\cdots11$, where a 0 corresponds to target absent and a 1 corresponds to target present in a cell. For example, consider the ninth hypothesis in a five-cell scenario. If we let S_i correspond to the target signal produced by the ith joint hypothesis, then the ninth hypothesis would be represented as H_{01001}, and the received signal contribution would be $S_{01001} = \mathbf{s}_4 + \mathbf{s}_1$.

The pdf under the ith joint hypothesis is given by

$$p(\mathbf{z} \mid H_i) = \frac{1}{\pi^N \sigma^{2N}} \exp\left(-\frac{1}{\sigma^2} (\mathbf{z} - S_i)^H (\mathbf{z} - S_i) \right). \tag{3}$$

In general the radar cannot observe each cell apart from the others. Thus, we must first update the joint hypotheses using Bayes' rule, which states that the posterior probability for each joint hypothesis is given by

$$P(H_i \mid \mathbf{z}_k) = \frac{P(H_i \mid \mathbf{z}_{k-1}) p(\mathbf{z}_k \mid H_i)}{p(\mathbf{z}_k)} \tag{4}$$

where $P(H_i \mid \mathbf{z}_{k-1})$ is the probability of the ith joint hypothesis prior to collecting the current (kth) measurement. While the denominator of (4) may not readily be available, it is the same for all joint hypotheses and serves only to normalize the probabilities such that they sum to unity. Thus, (4) simplifies to

$$P(H_i \mid \mathbf{z}_k) = \beta P(H_i \mid \mathbf{z}_{k-1}) p(\mathbf{z}_k \mid H_i) \tag{5}$$

where β can be computed after evaluating (4) for all joint hypotheses.

Now, we need the probability of joint hypothesis H_i prior to the kth measurement: $P(H_i \mid \mathbf{z}_{k-1})$. The length-$M$ probability vector that contains these probabilities prior to the kth measurement is

$$\mathbf{P}_{k-1} = [P_{M,k-1} \ldots P_{m,k-1} \ldots P_{1,k-1}]. \tag{6}$$

Let b_1 through b_M be the individual bits of the binary representation of a joint hypothesis. For example, the ninth joint hypothesis in the five-cell scenario described above would have $b_5 = 0$, $b_4 = 1$, $b_3 = 0$, $b_2 = 0$, $b_1 = 1$. Since target presence or absence is assumed to be independent across cells, the probability of the ith joint hypothesis is

$$P(H_i \mid \mathbf{z}_{k-1}) = \prod_{c=1}^{M} (P_{c,k-1})^{b_c} (1 - P_{c,k-1})^{1-b_c}. \tag{7}$$

Once a measurement $\mathbf{z}_k$ is received, it is used to update the probabilities for all joint hypotheses. First, 2^M likelihoods must be evaluated as dictated by (3). Then, all of the 2^M joint probabilities must be updated by (4), where (5) ensures summation to unity. Finally, the new cell probabilities are obtained through the marginal probabilities of the joint hypotheses. To calculate the marginal for the mth cell, we sum up the probabilities for any joint hypothesis that has a target-present state for that cell. The resulting sum is the updated probability for that cell. This approach can be extended to multidimensional probability maps, i.e., it can be applied to separable or ambiguous cells as illustrated in Fig. 2(a). The update procedure is summarized and illustrated in Fig. 3.

III. FORMATION OF A CRN TO DETECT AND TRACK MOVING TARGET WITH FOUR PARAMETERS

Transmitter spatial illumination strategies are dictated by predefined patterns. What makes the CR paradigm unique is that the transmit strategies and

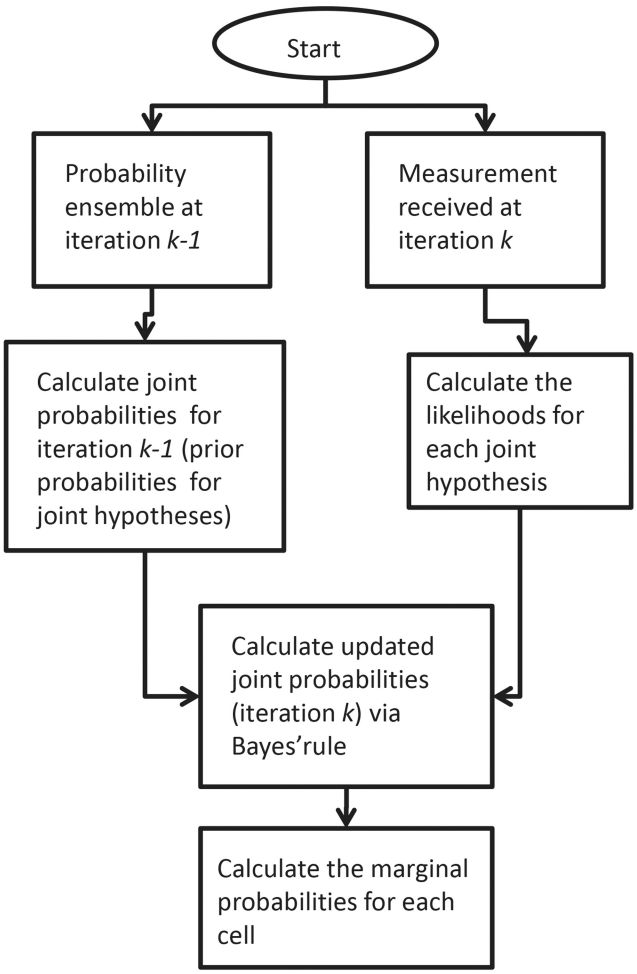

Fig. 3. Flow diagram of update procedure for updating cell probabilities.

receive processing are developed in a very integrated manner. Recall that the radar propagation channel is described probabilistically. Given time, probabilities may increase or decrease in each cell. Thus, a CR system must dynamically adapt the next interrogation to the continual changes in the propagation channel by processing both current measurements and prior probabilities. In a CR where a track function is required, tracking must also be incorporated. As such, a CR performing integrated-and-track functions should also include track priority in addition to the search priority in forming the next illumination strategy. It is our goal to build a CRN pictured in Fig. 1 that will be used for integrated search-and-track application and whose illumination strategy is matched to the radar environment. As mentioned the two radars cooperate in forming a dynamic spatial beamsteering strategy that responds to two competing priorities: 1) the continual search for targets and 2) the maintenance of target tracks. Here, we show that a compromise can be made that balances the two priorities by comparing the search uncertainty of the channel with the uncertainty of a target track. To this end we need to introduce uncertainty metrics such that this compromise can be performed. In Subsection A we introduce uncertainty measures for search-and-track via entropies. We need measurements in which to estimate position and velocities. Thus, in Subsection B, we relate the 4-D positional and velocity parameters to spatial and Doppler frequencies as measured by the two radars. We need signal models for the two radars, which is the topic of Subsection C. Of course the terrain of the physical surveillance area and the relative size the of the area being illuminated affect the probability updates and, as such, a scenario-specific probability model is introduced in Subsection D. Since the radar beam usually covers multiple cells and not just one cell, in Subsection E, we address how to quantify an entropy measure for a group of positional cells.

A. Entropy Measures of Search-and-Track Uncertainties

Entropy, which is a measure of uncertainty, is a function of a random variable's probability distribution [16]. Thus, to quantify the uncertainty of a target being in a cell, we may think of a single cell (in a probability ensemble regardless of size) as a binary random variable, where p is the probability of target presence and $1-p$ is the probability of target absence. Entropy is generally given by

$$h = \sum_{x} p(x) \frac{1}{\ln p(x)}. \tag{8}$$

We can apply (8) to each cell in the probability ensemble thereby creating a 4-D entropy map. However, spatial illumination is a 2-D function. Thus, we must collapse our 4-D entropy ensemble into a 2-D entropy map. Then, considering the search function, the CR can illuminate the area of most uncertainty. That is, the CR illuminates the region of the 2-D entropy map with the highest cumulative entropy. In Fig. 1 both radars are able to measure two positional dimensions and one velocity dimension. Radar A is not able to measure v_y, and radar B is not able to measure v_x, thereby producing the unique ambiguity problem discussed in Section II, where it was discussed that the probability map is nonetheless formed and updated despite this unique problem.

If we are to incorporate tracking into our illumination strategy, we also need the uncertainty of the track quality such that we can illuminate the target when this uncertainty becomes too high. The uncertainty of a track (assuming Gaussian parameters) depends on its covariance. The differential entropy of any Gaussian vector with covariance matrix $\mathbf{Y}$ is given by [16]

$$h_t = 0.5 \ln(2\pi e)^F \det(\mathbf{Y}) \tag{9}$$

where F is the dimension of the vector and $\det(\cdot)$ is the determinant of the matrix. It can now be seen how the track priority can be incorporated into the search

function; if the entropy h_t of a target exceeds an allowable level with respect to search entropy, then the CRN can interrupt the search function and illuminate the target. The track entropy is then reduced, i.e., the track covariance is tightened, and the search strategy resumes. Expanding on this idea we introduce a way to make a trade between the search-and-track functions by comparing the search entropy and the track entropy. It should be noted that the two entropies are of different types. To implement the desired priority balance, we introduce a scale factor to act as a dial between the two priorities.

B. Four-Dimensional Radar Channel

Consider Fig. 1 again. Each cell of the surveillance area describes a position in x,y space. If there are A cells in each position dimension, then there are A^2 position cells. Moreover, for each position cell, there are various (v_x,v_y) velocity possibilities. If there are B cells in each velocity dimension, then there are B^2 velocity cells. That is, there are $A^2 \times B^2$ total combinations of target position and velocity.

In radar the parameters of interest are directly related to signal frequencies. The physical position-and-velocity vector (x,v_x,y,v_y) corresponds to the observable spatial-and-Doppler frequency vector (k_x,d_x,k_y,d_y), where the relation between the two vectors is given by

$$(x,v_x,y,v_y) = (\alpha_1 k_x, \alpha_2 d_x, \alpha_3 k_y, \alpha_3 d_y) \tag{10}$$

i.e., $x = \alpha_1 k_x$, $v_x = \alpha_2 d_x$, $y = \alpha_3 k_y$, and $v_y = \alpha_4 d_y$, where the αs are scalars. The exact relationship between frequencies and parameters, i.e., the exact α values, depends on geometry and/or application but nonetheless have straightforward derivations. A popular example is the generic relation $f_d = 2v_d/\lambda_c$, where f_d is the Doppler frequency, v_d is the radial velocity, and λ_c is the frequency carrier wavelength [17]. For now it suffices to say that each parameter corresponds to a particular frequency as expressed in general form via the αs in (10).

Recall that in our application, a single radar measures three parameters, i.e., it is not able to measure velocity tangential to the radar-target line of sight. Consider Fig. 1 where the radars perform surveillance of the same area. To get a 4-D understanding, the two radars cooperate. Each radar has a 3-D cube of measurements after an illumination. The problem is how to use the two distinct 3-D measurement cubes to update a 4-D probability map. The update procedure in [15] is applied to solve this problem.

C. Signal Model For Two Radars

In active radar there are two ways in which a position can be measured. Range can be measured via temporal pulses (known as 'fast-time' sampling), while angle can be measured via antenna elements. In certain look-down geometries, target range can also be related to elevation angle, which can be measured with a vertical antenna array. Here, we use antenna elements in two dimensions to measure two target position coordinates. As shown in Fig. 1, both radars are able to measure the spatial frequencies k_x,k_y. Radar A is able to measure Doppler component d_x, and radar B is able to measure Doppler component d_y dimension. Considering radar A, the target signal (also called target steering vector) at a particular (k_x,d_x,k_y) is given by

$$\mathbf{s} = \mathbf{a} \otimes \mathbf{b}_x \otimes \mathbf{c} \tag{11}$$

where $\otimes$ is the Kronecker matrix product and

$$\mathbf{a} = \frac{1}{\sqrt{M_x}} \exp(j2\pi k_x [0 \cdots M_x - 1]^T) \tag{12}$$

$$\mathbf{b}_x = \frac{1}{\sqrt{N_x}} \exp(j2\pi d_x [0 \cdots N_x - 1]^T) \tag{13}$$

$$\mathbf{c} = \frac{1}{\sqrt{M_y}} \exp(j2\pi k_y [0 \cdots M_y - 1]^T) \tag{14}$$

where $0,1,\ldots,M_x-1$ are antenna element indices for measuring k_x; $0,1,\ldots,N_x-1$ are the temporal indices for measuring d_x; and $0,1,\ldots,M_y-1$ are the antenna element indices for measuring k_y, respectively.

Let q be the index of the targets present in the scene, i.e., $q \in (1,\ldots,Q)$, and $\mathbf{s}^{(q)}$ be the steering vector that corresponds to the qth target. Let the 2-D transmit beam pattern S, whose main beam is centered on some (x,y) in the physical space, be described by $S(k_x,k_y)$. For convenience we assume that the main beam gain is constant, and we ignore the contributions of the sidelobes. If we let $\eta^{(q)}$ be the complex reflection of a target in the qth cell, then the received steering vector due to this target is given by

$$\mathbf{v}^{(q)} = \eta^{(q)} S(k_x,k_y) \mathbf{s}^{(q)}. \tag{15}$$

As mentioned previously radar systems operate in clutter environments. Let the noise be $\mathbf{w} \sim \mathcal{CN}(\mathbf{0},\mathbf{R})$, where $\mathbf{R} = \sigma^2\mathbf{I} + \mathbf{C}_c$ is the covariance matrix that results from both additive white Gaussian noise (AWGN) and clutter interference. In our application the two radar platforms are static, such that clutter is centered at zero Doppler. In practice, however, clutter is shown to have some Doppler spread due to intrinsic clutter motion that occurs even for stationary radars. We assume that the clutter covariance $\mathbf{C}_c$ is known. The total signal contribution due to Q targets is given by $\mathbf{v} = \sum_{q=1}^{Q} \mathbf{v}^{(q)}$, and the measurement $\mathbf{z}$ is given by $\mathbf{z} = \mathbf{v} + \mathbf{w}$. Then, the measurement becomes

$$\mathbf{z} = \sum_{q=1}^{Q} \eta^{(q)} S(k_x,k_y) \mathbf{s}^{(q)} + \mathbf{w}. \tag{16}$$

Considering radar B the target steering vector at a particular (k_x, d_x, k_y) is given by

$$\mathbf{s} = \mathbf{a} \otimes \mathbf{d}_y \otimes \mathbf{c} \tag{17}$$

where $\mathbf{a}$ and $\mathbf{c}$ are from (12) and (14) and where

$$\mathbf{d}_y = \frac{1}{\sqrt{N_y}} \exp(j2\pi d_y [0 \cdots N_y - 1]^T). \tag{18}$$

Clearly, $0, 1, \ldots, N_y - 1$ are the temporal indices for measuring d_y. Notice (15) and (16) also apply for radar B.

D. Dynamic Probability Model

Now consider Fig. 4, which represents the physical surface under surveillance by the CRN. While a small area is being illuminated by the main beam, targets may appear in unilluminated areas such that the cell probabilities in those areas change dynamically. In other words the uncertainty of a target being present (or absent) in an unilluminated cell adjusts to a value that is reflective of some steady-state probability of the cell. Hence, there is a need to model the probability changes for the unilluminated cells during interrogation. Thus, in our simulations, a dynamic probability model which reflects a cell's increase/decrease toward a steady-state probability is implemented. The steady-state probabilities may not be equal for all cells because they may be scenario-dependent due to areas of the scene that are more likely to be occupied or traveled by moving objects or targets. For example, let a particular area be a land area containing three major features. Ordered in increasing difficulty for travel, they are: 1) dirt road, 2) coarse ground, and 3) rocky ground. In reality, the area may be part of an outback park, where all types of vehicles are allowed to pass through to any part of the area. It is likely that most of the vehicles will travel the dirt roads for ease. Clearly, the dirt roads should have the highest steady-state probabilitie,s while the rocky grounds should have the lowest steady-state probabilities. Because the area has different steady-state probabilities, such an area may be termed heterogeneous. Exact steady-state probabilities are usually unknown a priori, but clearly a model reflecting a scenario like the example above could be constructed using land-use and land-feature models. If indeed our goal is to build a CRN, then the dynamic probability model should reflect dynamic uncertainty changes, which can be used by each radar to revisit various areas it has already illuminated since probabilities in those areas can change over time.

For the purposes of illustration of our CR network, all cells will be considered homogeneous, meaning that all cells will converge to the same steady-state probability. Of course, this simplistic assumption may be not true in practice, and this simplistic model is only used for simulation purposes. Also, in our

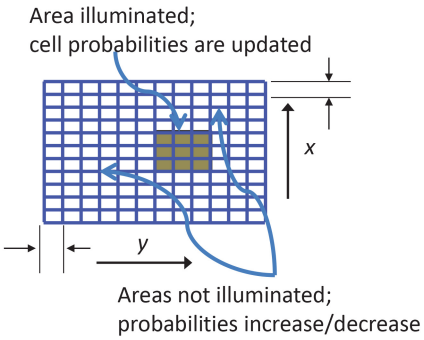

Fig. 4. Probabilities are updated in illuminated areas via measurements. For nonilluminated cells, dynamic probability model can be used.

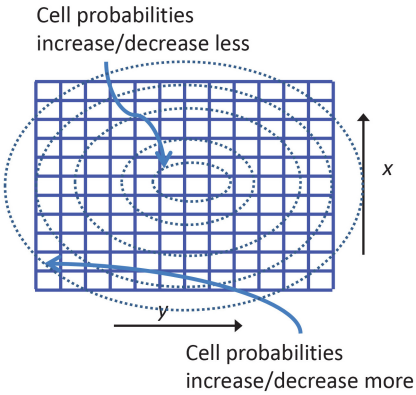

Fig. 5. In this dynamic probability model, large concentric circles indicate higher rates of convergence towards steady-state values.

scenario, we assume that targets are more likely to enter the scene through the boundaries of the scene rather than appearing in the interior of the scene. Referring to Fig. 5 the concentric circles indicate that the outside probabilities converge more rapidly to their steady-state probabilities, which reflects the fact that the scene is more dynamic near its boundaries. That is, when the cells are not being illuminated, the probability rate of increase/decrease of an outside cell is greater than that of an inside cell. Again, it should be noted that probability models are scenario-dependent and that a good model depends on a good understanding of the physical terrain as well as of target behaviors.

E. Bit Entropy as Natural Measure of Target Cell Uncertainty

For a particular cell the cell entropy (CE) (8) becomes

$$h_c = -p \log_2 p - (1-p) \log_2 (1-p) \tag{19}$$

which is said to have units in bits. It is the well-known binary random variable entropy in Shannon's classical work [18], where $p = 0.5$ corresponds to the maximum uncertainty and $p = 0$ and $p = 1$ correspond to no uncertainty. If the cell does not get illuminated as shown in Fig. 4, the

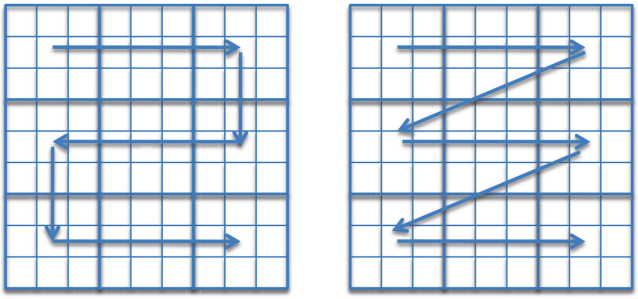

Fig. 6. Traditional beamsteering strategies usually employ rasterized-type patterns.

uncertainty should move towards its steady-state uncertainty. If it gets illuminated then the cell gets an updated probability value via the method in Section II, and the new uncertainty value is easily calculated via (19). If a cell has a probability of 0.5, it achieves the maximum CE of 1 bit. Typically, the sensor beamwidth covers an area (the area of a beam position) greater than just one cell, and, thus, we are interested in the uncertainty of a group of cells. To get an entropy value for a particular beam position, we sum the individual CEs of the illuminated cells.

IV. BEAMSTEERING STRATEGIES

A. Traditional Search Beamsteering Strategy

In practice the desired surveillance area is very large. Figure 6 shows how the traditional or rasterized beamsteering strategy works. The beam scans to cover the full area. We define a beam position to be the group of cells covered by a beamwidth. We make a simplifying assumption that a square area is illuminated by the main beam. In the rasterized search strategy, the idea is to place the beam into the first beam position (which is the left top-most portion of the total area of the first row in Fig. 6), receive measurements, and then place it in the next or adjacent beam position. When it reaches the end of the first beam row, the beam is placed in the beam position below it, which is in the second row. A variation is also shown in Fig. 6. However, this fixed conventional scanning strategy may be improved by matching the beamsteering to a measure of uncertainty.

B. Adaptive Search-Only Beemsteering Strategy Based on Area Uncertainty

At any point in time, a good strategy for a CR is to place the beam in the location that provides the most reduction in uncertainty via data collection, which is directly related to mutual information (MI) [16]. However, we have a 4-D probability ensemble, and the spatial beam is a function of a 2-D pattern. We have to reduce the corresponding 4-D entropy ensemble by collapsing it into a 2-D entropy map that corresponds to the 2-D physical area (x,y). First, we calculate the target CEs as dictated (19). To collapse the 4-D map to a 2-D map over (k_x,k_y) dimensions, we average over the Doppler frequencies as given by

$$h_c(k_x,k_y) = \frac{1}{B_x B_y}\sum_{j=1}^{B_x}\sum_{i=1}^{B_y} h_c(k_x,d_x,k_y,d_y). \quad (20)$$

Equation (20) is the 2-D entropy map corresponding to our surveillance area and is clearly a function of the spatial frequencies. If the total number of cells in a beam position is C, then the beam position entropy (BPE) is simply given by

$$h_P = \sum_{u=1}^{C} h_{c,(u)}(k_x,k_y) \quad (21)$$

where u serves as a cell index in a beam position and $h_{c,(u)}$ is the corresponding CE via (20). If the total possible number of beam positions within the surveillance area is K, then we calculate K different entropy values, one for each beam position. To match to the search area of most uncertainty, the CR system illuminates the beam position with the largest h_P. Next, the CR again recalculates the BPEs and again illuminates the beam position with the largest BPE. The cycle continues until a detection occurs and a track is established. Once a track is established, a compromise must be made between the search and track functions.

V. ADAPTIVE SEARCH-AND-TRACK BEEMSTEERING STRATEGY

Closed-loop operation is one of the defining characteristics of a cognitive system, i.e., CR dynamically responds to its environment. Another is the ability to account for inputs or commands critical to the objectives of a system, such as mission priorities. Here, we develop a two-platform CR system that is able to perform two task priorities (search and track) that compete for the spatial illumination (beamsteering) resource. We introduce a way for the CR to take in input that dictates the prioritization between search and track functions. If we are to perform tracking, we need a motion model. In addition, we need an initial estimate of the target parameters and a prediction of the next parameter values as targets move. In our application we use the the well-known Kalman tracker, which is presented in [19], as the optimal solution for target parameter estimation in a Bayesian context.

A. Motion Model

In our motion modeling and tracking, we track k_x and k_y and their corresponding spatial frequency velocities v_{k_x} and v_{k_y}, which are given by $v_{k_x} = (1/\epsilon_1)d_x$ and $v_{k_y} = (1/\epsilon_2)d_y$, respectively, where $1/\epsilon_1 = \alpha_1/\alpha_2$ and $1/\epsilon_2 = \alpha_3/\alpha_4$ via (10). Let $\mathbf{r}_i$ be

the state vector of true target parameters given by $\mathbf{r}_i = [k_x \;\; v_{k_x} \;\; k_y \;\; v_{k_y}]^T$, where i is the current time step. Let $\triangle T$ be the time step between illuminations by either radar. Then, defining the transition matrix $\mathbf{A}$ to be

$$\mathbf{A} = \begin{bmatrix} 1 & \triangle T & 0 & 0 \\ 0 & 1 & 0 & 0 \\ 0 & 0 & 1 & \triangle T \\ 0 & 0 & 0 & 1 \end{bmatrix} \tag{22}$$

the updated target state vector is $\mathbf{r}_{i+1} = \mathbf{A}\mathbf{r}_i$. While we have addressed the probability updates for parameter cells, we have not yet addressed the estimates of true parameters such that target tracking can be established. Let the estimated state vector be $\hat{\mathbf{r}}_i = [\hat{k}_x \;\; \hat{v}_{k_x} \;\; \hat{k}_y \;\; \hat{v}_{k_y}]^T$. Then, the motion model becomes $\hat{\mathbf{r}}_{i+1} = \mathbf{A}\hat{\mathbf{r}}_i + \mathbf{q}$, where $\mathbf{q} \sim \mathcal{N}(\mathbf{0}, \mathbf{Q})$ represents the variation in target maneuvers as a zero-mean Gaussian process with a covariance matrix of $\mathbf{Q}$.

B. Target Parameter Estimation

Initializing a track requires estimating target parameters of interest, but the detecting radar is blind to one of the Doppler frequencies. As such, the target parameter vector $\mathbf{r}$ involves only three of the frequencies of interest. Let's consider a detection by the radar that is able to measure the d_x frequency. For example and simulation purposes, assume a target model where target amplitude is known, then the pdf of the measurement $\mathbf{z}$ is given by

$$\begin{aligned} p(\mathbf{z}; k_x, \epsilon_1 v_{k_x}, k_y) = {} & \frac{1}{\pi^N \det(\mathbf{R})} \\ & \times \exp[-(\mathbf{z} - \mathbf{s}(k_x, \epsilon_1 v_{k_x}, k_y))^H \mathbf{R}^{-1} \\ & \times (\mathbf{z} - \mathbf{s}(k_x, \epsilon_1 v_{k_x}, k_y))]. \end{aligned} \tag{23}$$

We desire to find a vector estimate that maximizes the above likelihood. It is shown in the Appendix that this is equivalent to

$$\min_{k_x, v_{k_x}, k_y} [\mathrm{Re}\{\mathbf{z}^H \mathbf{R}^{-1} \mathbf{s}(k_x, \epsilon_1 v_{k_x}, k_y)\}]. \tag{24}$$

Note the absence of spatial frequency velocity v_{k_y} since the radar is blind to d_y frequency. For an initial estimate of target parameters, we have the choice of any of the velocities within the cell of detection, or we may choose the center of the detected cell. For the purposes of demonstrating our CR framework via simulation, we form parameter estimates using the asymptotic properties of the MLE. For large data sets it is shown [20] that the MLE is unbiased, i.e., that the mean of the estimates are equal to the true parameters. Moreover, the MLE is asymptotically Gaussian distributed, and the covariance is approximately equal to the Cramer-Rao lower bound (CRLB). That is, the estimated target parameters are Gaussian-distributed according to

$$\hat{\mathbf{r}} \sim \mathcal{N}(\mathbf{r}, \mathbf{J}^{-1}(\mathbf{r})) \tag{25}$$

where $\mathbf{J}^{-1}$ is the inverse of the Fisher information matrix (FIM) and is equal to the CRLB covariance. We can produce useful parameter estimates for simulation purposes without a full numerical search by taking realizations as dictated by (25). The covariance is given by $\mathbf{C}(\hat{\mathbf{r}}) = \mathbf{J}^{-1}$. In [21] it is noted that each element of the FIM is given by

$$J_{ij} = \mathrm{Tr}\left[\mathbf{R}_C^{-1} \frac{\partial \mathbf{R}_C^{-1}}{\partial \mu_i} \mathbf{R}_C^{-1} \frac{\partial \mathbf{R}_C^{-1}}{\partial \mu_j}\right] + 2\,\mathrm{Re}\left[\frac{\partial^H \boldsymbol{\mu}}{\partial \mu_i} \mathbf{R}_C^{-1} \frac{\partial \boldsymbol{\mu}}{\partial \mu_j}\right] \tag{26}$$

where $\mathrm{Tr}(\cdot)$ stands for the trace of a matrix and $\mathrm{Re}(\cdot)$ stands for a real part of a complex number. $\boldsymbol{\mu}$ and $\mathbf{R}_C$ are the mean and covariance matrix of the measurement, respectively. Here, we consider the approach to get estimates for four parameters. In our simulation we assume that the covariance is known and that $\boldsymbol{\mu}$, the mean steering vector, is given by

$$\mu = S(k_x, k_y) \tilde{\mathbf{s}}(k_x, v_{k_x}, k_y, v_{k_y}) \tag{27}$$

where $S(k_x, k_y)$ is the antenna gain and the steering vector is given by

$$\tilde{\mathbf{s}}(k_x, v_{k_x}, k_y, v_{k_y}) = \mathbf{a} \otimes \mathbf{b} \otimes \mathbf{c} \otimes \mathbf{d} \tag{28}$$

where $\mathbf{a} = [0 \;\; \exp(j(1)2\pi k_x) \cdots \exp(j(M_x - 1)2\pi k_x)]^T$, $\mathbf{b} = [0 \;\; \exp(j(1)2\pi v_{k_x}) \cdots \exp(j(N_x - 1)2\pi v_{k_x})]^T$, $\mathbf{c} = [0 \;\; \exp(j(1)2\pi k_y) \cdots \exp(j(M_y - 1)2\pi k_y)]^T$, and $\mathbf{d} = [0 \;\; \exp(j(1)2\pi v_{k_y}) \cdots \exp(j(N_y - 1)2\pi v_{k_y})]^T$. The individual FIM entries needed for the CRLB are

$$\begin{aligned} J_{11} = {} & 2S^2 \\ & \times \mathrm{Re}\left\{\left[\frac{\partial \mathbf{a}}{\partial k_x} \otimes \mathbf{b} \otimes \mathbf{c} \otimes \mathbf{d}\right]^H \mathbf{R}_C^{-1} \left[\frac{\partial \mathbf{a}}{\partial k_x} \otimes \mathbf{b} \otimes \mathbf{c} \otimes \mathbf{d}\right]\right\} \\ & \vdots \\ J_{44} = {} & 2S^2 \\ & \times \mathrm{Re}\left\{\left[\mathbf{a} \otimes \mathbf{b} \otimes \mathbf{c} \otimes \frac{\partial \mathbf{d}}{\partial v_{k_y}}\right]^H \mathbf{R}_C^{-1} \left[\mathbf{a} \otimes \mathbf{b} \otimes \mathbf{c} \otimes \frac{\partial \mathbf{d}}{\partial v_{k_y}}\right]\right\}. \end{aligned} \tag{29}$$

Due to the length of (29), the rest of the equation list is not shown here. The reader is referred to [22]. While (29) seems formidable it is easily evaluated. When these individual entries are calculated, the FIM is formed, and the CRLB is found by taking its inverse. Note that the CRLB is inversely proportional to S^2, the square of spatial pattern gain, i.e., the errors are smaller for larger antenna gain due to an increase in signal-to-noise ratio (SNR). This approach of taking a random draw as an estimate produces relatively equivalent statistical models for parameter

estimation errors as the MLE [12]. We can now use (25) to obtain initial estimates of the parameters once detection is declared. Tracking can now commence, which is the subject of the next section.

C. Kalman Tracking and Target Track Entropy

In our application we use the Kalman tracker, which was presented in [23] as the optimal solution for target parameter estimation in a Bayesian context. The Kalman tracker is clearly integral to our application, but it is not the focus of this work, and as such, only the pertinent equations are presented here. We refer the interested reader to the excellent treatment in [20].

First, let $\hat{\mathbf{r}}$ be the initial vector estimate of the parameters that is based on MLE and generated with a realization using the CRLB $\mathbf{C}(\hat{\mathbf{r}})$. The initial error covariance is $\mathbf{P} = \mathbf{C}$. Violation of this assumption, clearly, may affect subsequent estimates. For simulation purposes we make this our initial assumption. The prediction for the next state is $\hat{\mathbf{r}}_{i+1} = \mathbf{A}\hat{\mathbf{r}}_i$, and the prediction covariance matrix (PCM) is $\mathbf{P}_{i+1} = \mathbf{A}\mathbf{P}_i\mathbf{A}^T + \mathbf{Q}$, where $\mathbf{Q}$ is the covariance of the target maneuverability given by

$$\mathbf{Q} = \begin{bmatrix} 0 & 0 & 0 & 0 \\ 0 & \sigma^2_{v_{k_x}} & 0 & 0 \\ 0 & 0 & 0 & 0 \\ 0 & 0 & 0 & \sigma^2_{v_{k_y}} \end{bmatrix}. \tag{30}$$

The Kalman gain matrix (KGM) is $\mathbf{K} = \mathbf{P}_i(\mathbf{C} + \mathbf{P}_i)^{-1}$, where the updated state vector or correction is given by $\hat{\mathbf{r}}_i = \hat{\mathbf{r}}_i + \mathbf{K}(\mathbf{u} - \hat{\mathbf{r}}_i)$ and $\mathbf{u}$ is the vector with true parameters plus noise. Then, the state covariance matrix (SCM) is given by

$$\mathbf{P}_i = (\mathbf{I} - \mathbf{K})\mathbf{P}_i \tag{31}$$

which represents the covariance of the target state vector after an illumination. Thus, the SCM grows when the target is not illuminated. Clearly, the quality or "tightness" of the track depends on the tracked target's SCM in (31). Using (9) our system's target track entropy (TTE) is given by

$$h_t = 0.5\ln(2\pi e)^4 \det(\mathbf{P}). \tag{32}$$

The TTE plays an important role in the formation of an adaptive integrated search-and-track beamsteering strategy for the CR system, which is the topic of the next subsection.

D. Adaptive Integrated Search-and-Track Beamsteering

There are two aspects of the CR system in which the search function and track function will be truly integrated. One is in propagation of probabilities of tracked targets. Due to motion a tracked target will eventually move into a nearby cell. Our probability updates do not account for target motion and, therefore, are inadequate in incorporating the fact that a target may have or has moved into a nearby cell. Via the Kalman filter the CR network predicts the next position for the tracked target. If the next predicted position crosses a cell boundary, then the CR uses this knowledge to shift the high probability associated with the target to the new cell. The resulting predictive nature of the CR via the integration of the Kalman filter allows for propagation of the cell probability associated with the tracked target. The Kalman filter alone does not consider cell probabilities, and Bayes' rule does not account for the motion of targets across cells. But the CR framework, which integrates cell probabilities with tracking, has this unique capability not available in conventional radar systems. The other aspect is how to balance the two priorities that compete for the spatial beamsteering resource. The search priority dictates the beamsteering strategy such that the search uncertainty is reduced. In other words the search priority strategy is for the CR to detect as many moving targets as it can before they leave the scene. On the other hand the track priority dictates the CR to frequently illuminate the beam on the target such that a high-quality track is maintained.

We have CE as a measure of uncertainty of a cell (19) and TTE as a measure of track uncertainty as given by (32). In one illumination we only cover one beam position. The BPE is given by (21). As pointed out earlier with the "adaptive search-only" approach, we can calculate all the possible beam position entropy values and choose to put the next beam to the position with the maximum BPE. To integrate our track priority, a straightforward way is to monitor the TTE. When the TTE becomes high such that the track quality needs to be maintained (that is, SCM has grown and needs to be tightened), the CR system needs to place the next beam on the tracked target. A novel idea is to somehow compare the TTE with the maximum BPE and, when the TTE is larger in some sense than the BPE, then the "adaptive search-only" is interrupted to accommodate the track priority, and the beam is moved to the tracked target. It is not apparent how one compares TTE with BPE since they are different entropy types. The TTE is an uncertainty metric involving target parameters that can take on continuous values, while the BPE is an uncertainty metric accumulated over many binary random variables. The TTE is measured in nats. The BPE is measured in bits, whose maximum value is C bits, which is the number of cells C in the beam position times the maximum CE of 1 bit. Here, we propose using a scaling factor Ω that renders both entropy types to be comparable, i.e.

$$\Omega h_t \sim h_P \tag{33}$$

where the symbol $\sim$ means that the entropies in (33) are in the same order of magnitude. Thus, considering a single tracked target, the illumination strategy rule is

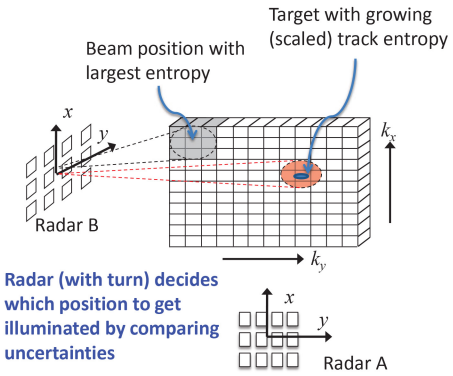

Fig. 7. Uncertainties due to search area and tracked target. Radar with turn decides which beam position to illuminate by comparing BPE and TTE.

given by

$$\begin{aligned} &\text{if} \quad h_t > \frac{h_{P,\max}}{\Omega} \text{ then illuminate target} \\ &\text{else} \quad \text{illuminate area with max BPE} \end{aligned} \tag{34}$$

where $h_{P,\max}$ is the maximum BPE over all possible beam positions at the current time. The situation is shown in Fig. 7, where a TTE grows over time when not illuminated and the radar/s must update to curtail the growth of the track uncertainty. This approach has worked very well. That is, by changing the value of Ω, the CR network is able adjust the emphasis as to which function to prioritize. Indeed, Ω becomes an input to the CR system that controls the overall system preference between search and track priorities; a useful feature for any practical radar system. Once Ω is initialized the CR system will operate in a closed-loop manner but tries to maintain the balance between priorities as dictated by Ω. A good starting value for Ω is to look at the desired track quality requirement. In other words we have an SCM to maintain or a desired TTE, then we scale TTE (with Ω) such that the scaled TTE is C bits or less (since C is the maximum possible BPE). With this method it can be said that the CRN employs an "adaptive integrated search-and-track" beamsteering strategy. In the next section we present example applications of the CRN that we just built.

VI. SIMULATION AND PERFORMANCE RESULTS WITH INTEGRATED SEARCH-AND-TRACK CRN

In the last section we developed all the necessary models to build a two-platform CR network that accommodates the priority needs as dictated by the search-and-track functions of a radar system that performs ground surveillance with a four-parameter target track. Before simulation results for various scenarios are presented, it is worthwhile to review the operational framework of our CRN.

The operational framework is best described by Fig. 8. Note the necessarily closed-loop nature of the CR network. First, the system user inputs Ω, which represents the priority scale that the CRN uses to dial search-and-track priorities. Then, initial prior probabilities are set for all the cells in the 4-D probability ensemble. During initialization neither radar illuminates the scene. We assume the use of the dynamic probability model after the priors are set. The CR system calculates BPE for all beam position possibilities, finds the maximum, and

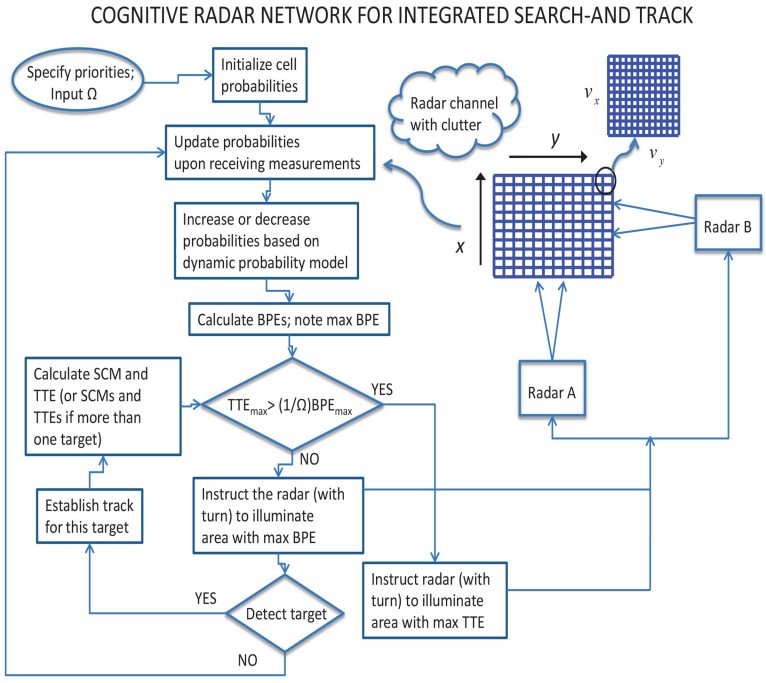

Fig. 8. Two-platform CRN for ground surveillance performing integrated search-and-track of moving targets.

notes the beam position location. If no targets are detected, any TTE is initialized to zero. The CRN instructs radar A (assuming that radar A starts) to illuminate the beam position with the highest BPE, and as such, the search function commences. Radar A receives the measurements and passes them to the CR processor. The CR processor processes the measurements and updates the 4-D probability map. It should be mentioned that the CR processor may actually reside in either radar or be a separate unit. The actual location of the CR processor depends on the hardware capability of the system and/or the individual radar sensors. The proper allocation strategy of the processing functions is interesting but is not discussed further. Once the probabilities are updated, they are compared with the detection probability threshold. If a cell has a probability greater than the threshold, detection is declared, and a track is established. The CRN calculates the TTE for this target. If this TTE is greater than the $1/\Omega$-scaled maximum BPE as dictated by (34), then the CRN instructs radar B to illuminate the target; otherwise it illuminates the position with maximum BPE. If the radar illuminates the tracked target, then the center of the beam is placed on the target's cell, except when the target is in the corner or on the edges. In these cases the beam is placed such that the target is inside it. Then, radar B receives the signal returns. The CRN updates the probabilities, check for detections, and establishes tracks for detected targets, and the cycle continues. If there are now multiple tracks, then the CR calculates for the maximum TTE and notes the location of the corresponding target. If (34) is met then the radar (with turn) illuminates the target. Clearly, the procedure continues, and a method for the CRN to decide which function to be prioritized at any time in its operation is in place. As noted this beamsteering strategy is real-time and is dynamically matched to the channel (search and track) uncertainties.

A. Track Example for Adaptive Search-and-Track

For all the examples throughout this paper, the spatial and Doppler frequencies are normalized, i.e., $-0.5 < k_x < 0.5$, $-0.5 < d_x < 0.5$, $-0.5 < k_y < 0.5$, and $-0.5 < d_y < 0.5$. We pick ϵ_1 and ϵ_2 to be -5 such that

$$d_x = -5v_{k_x} \tag{35}$$

$$d_y = -5v_{k_y}. \tag{36}$$

Then, $-0.1 < v_{k_x} < 0.1$ and $-0.1 < v_{k_y} < 0.1$. The variances of the spatial frequency velocities are set at 1e-7, and the timestep is set at 0.0025. Both radars operate in clutter environments, where each clutter power spectral density (PSD) is lowpass-shaped and is centered at 0 Hz. The clutter-to-noise ratio (CNR) is set at 30 dB. The number of antenna elements for spatial measurements are $M_x = 3$ and $M_y = 3$, and the number of filter taps for Doppler measurements are $N_x = 15$ and $N_y = 15$.

In our scenario examples the target is initially located in or near cell 1; more specifically, the target starts at $k_x = -0.45$, $v_{k_x} = 0.085$, $k_y = -0.45$, and $v_{k_y} = 0.085$. The CRN uses the adaptive integrated search-and-track strategy developed in the last section. The illumination update rate, the rate in which a tracked target is illuminated, is set to the rate that would result if the rasterized scanning strategy were used. The scenario size for this experiment is such that the cell sizes for the spatial frequency k_x, the spatial frequency velocity v_{k_x}, the spatial frequency k_y, and the spatial frequency velocity v_{k_y} are $A_x = 30$, $B_x = 15$, $A_y = 30$, and $B_y = 15$, respectively. Figure 9 shows the track for the k_x and k_y parameters, and Fig. 10 shows the track for the v_{k_x} and v_{k_y} parameters. The left-hand panel shows the track for the entire duration of the target's motion. That is, it shows the track from the moment the target was detected until it left the scene. Illumination 1 is not the first illumination or time step when the target appeared in the scene but rather corresponds to the estimated location of the target when it was first detected. The right-hand panel shows the track for the first 1000 time steps (illuminations) and zoomed close-in to show the granularity of the track. Note from the initial parameters of the target, that it was set to start near the northwest corner of the scene, travel across the scene, and leave the scene somewhere in the southeast corner. In terms of position, notice from Fig. 9, that the target was detected when it was at $(-0.2686, -0.2923)$ and the initial estimate was $(-0.2623, -0.2990)$. The target left the scene at location $(0.4998, 0.2541)$, and the last estimate was $(0.5009, 0.2567)$. Thus, it was detected between its starting location and the origin $(0.0000, 0.0000)$, i.e., it was detected early in its course of motion.

B. Beam Accumulation Histories with Increasing Ω

We had mentioned that a way for the CRN to dictate the importance of a track priority as opposed to the search priority is through the use of the priority dial Ω. We consider a fairly large scenario size of 60-by-15-by-60-by-15. We consider experiments in which we change the value of Ω and observe the effects on track quality as a function of increasing Ω. More interestingly we look at the beam accumulation histories as a function of increasing Ω. Beam accumulation history is simply a picture of the whole surveillance area that shows the number (or density) of illuminations spent on each cell of the surveillance area in the course of an experiment. First, it should be clear that the beam accumulation history for the rasterized beamsteering strategy would be uniform and, therefore, uninteresting.

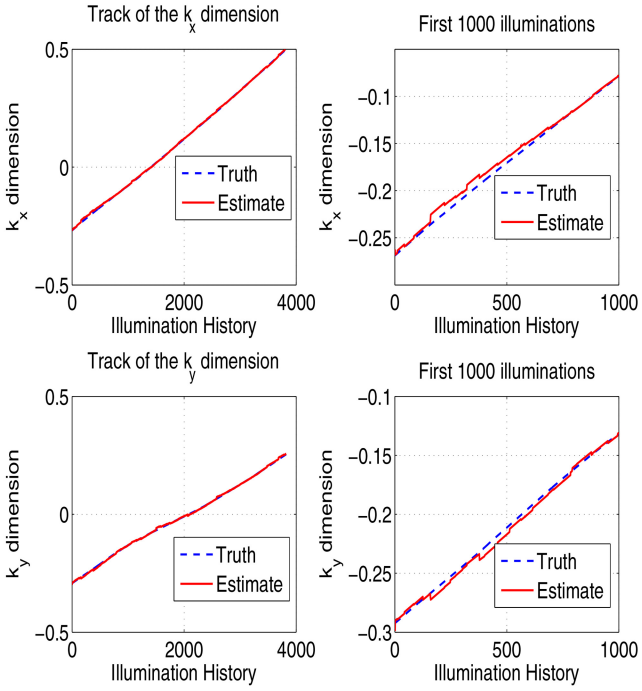

Fig. 9. Position tracks of example scenario using adaptive integrated search-and-track with scenario size of 30-by-15-by-30-by-15. Left panel shows entire track history. Right panel shows first 1000 time steps as soon as track is established and zoomed close-in to show track granularity.

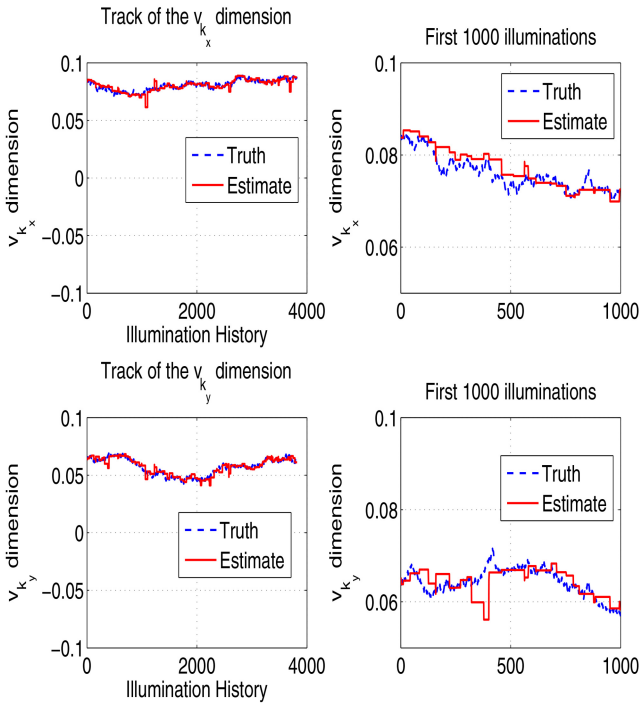

Fig. 10. Velocity tracks of example scenario using adaptive integrated search-and-track with scenario size of 30-by-15-by-30-by-15. Left panel shows entire track history. Right panel shows first 1000 time steps as soon as track is established and zoomed close-in to show track granularity.

In this scenario size the $\Omega = 0$, $\Omega = 1e20$, and $\Omega = 5e20$ values are used. The value of $\Omega = 0$ means that track quality is ignored. The value of $\Omega = 1e20$ corresponds to a small increase in track priority, and the value of $\Omega = 5e20$ represents the highest track priority. It should be clear that the values of the Ωs would actually correspond to different illumination update rates once a track is detected. Figure 12 contains the beam accumulation histories corresponding to the use of the three Ωs. The target was detected between the origin and the southeast corner of the scene. The beam accumulation history corresponding to $\Omega = 0$ (top panel) clearly reflects the CRN's attempt to match the search uncertainty with no regard to the target track, while the beam accumulation history corresponding to $\Omega = 1e20$ reflects some emphasis on the target track, where an increase in the accumulation density around the southeast corner of the scene can be discerned. The bottom panel corresponds to the beam accumulation history that employs $\Omega = 5e20$. Here, the pronounced streak near the southeast corner of the scene clearly indicates that the target was detected between the origin and the southeast corner of the scene and that the track priority emphasis is significant.

Note also the "concentric" circular contour of the beam histories. This is due to the fact that the beamsteering strategy was matched to the dynamic probability model of our scenario that was discussed in Section III. The case of $\Omega = 0$ is really the adaptive search-only strategy, and it is very clear in Fig. 12 that the beams are concentrated on the outside cells rather than the inside. For the $\Omega = 1e20$ and the $\Omega = 5e20$ cases, the adaptive search-and-track beamsteering strategy is formed such that the channel uncertainty is reduced while maintaining an illumination update rate for the tracked target. Figure 11 shows the positional tracks for the three sample experiments. The left panel shows tracks for the k_x position, and the right panel shows tracks for the k_y position. From the moment of establishing track for this target, there were about 750 time steps (illuminations) until the target left the scene. For brevity velocity tracks are not shown. As expected there is an improvement in track quality going from $\Omega = 0$ to $\Omega = 1e20$ since the illumination updates are more frequent for $\Omega = 1e20$ than for $\Omega = 0$. The track quality improvement for $\Omega = 5e20$ is clearly the best among the three because of the highest illumination update rate. The increasing target track quality intuitively matches the corresponding beam accumulation histories.

C. Performance Simulation

Finally, we want to gauge the detection performance of the two-platform CRN employing adaptive search-and-track beamsteering strategy compared with a system with two radars, each of which employ the traditional rasterized beamsteering strategy. For fair comparison the illumination update rates for both systems are set to be

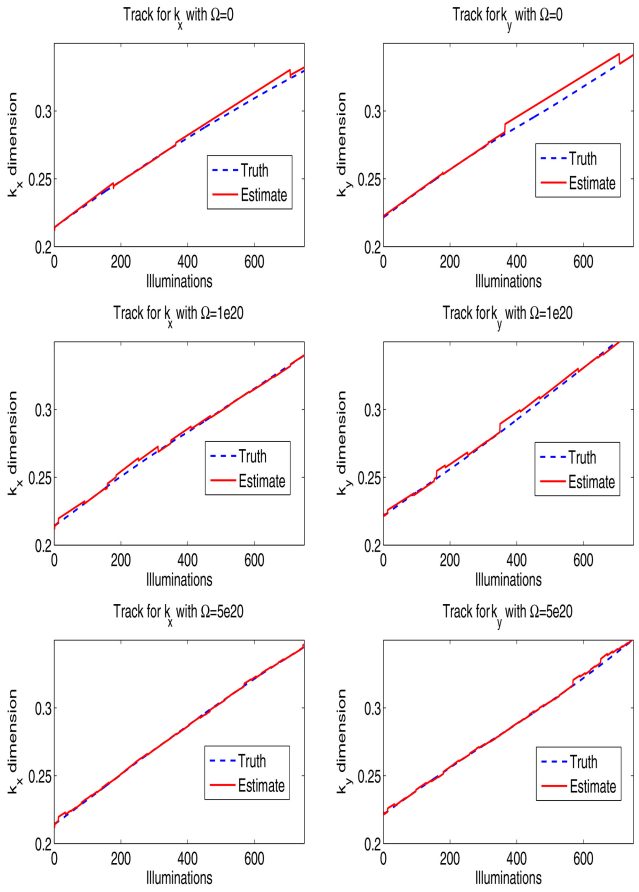

Fig. 11. Positional tracks (k_x,k_y) for scenario size 60-by-15-by-60-by-15 for different values of Ω. Top panel: Ω = 0. Middle panel: Ω = 1e20. Bottom panel: Ω = 5e20.

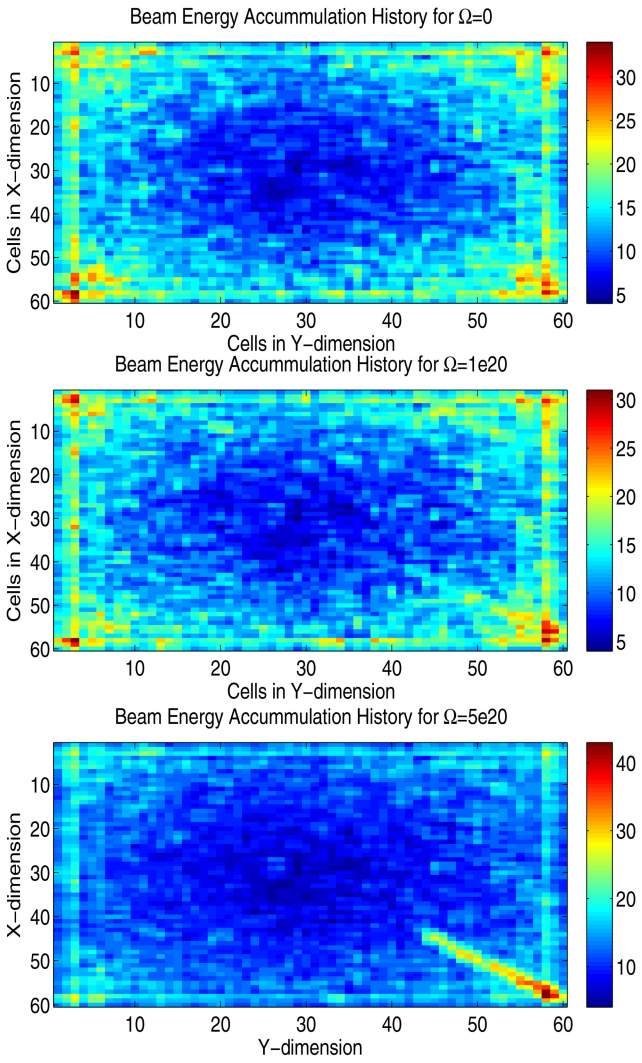

Fig. 12. Beam energy accumulation histories for scenario size 60-by-15-by-60-by-15 for different values of Ω. Top panel: Ω = 0. Middle panel: Ω = 1e20. Bottom panel: Ω = 5e20.

equal. The detection performance is calculated via Monte Carlo simulation, and the detection performance is over increasing SNR. We consider two manageable scenarios of 24-by-15-by-24-15 and 30-by-15-by-30-15. For each SNR there are 20 Monte Carlo trials. For each trial we allow for 25 targets to appear in the scene. That is, for each SNR, there are a total of 500 targets in which to average detection performance. To conveniently ensure the illumination update rates are equal, we let only a maximum of two targets move in the scene at a time. That is, when one target leaves, we allow one target to appear, while another target is potentially being detected or tracked. The starting positions and velocities of the targets are random but with slight restrictions on the positions and velocities. Recall that our dynamic probability model dictates that the targets are more likely to appear on the edge or in the corners. Thus, we allow for the targets to take initial positions at random edges when they first appear in the scene. To keep the simulation time manageable, we allow for targets to take on all possible velocity values except the ones near 0 Hz. Those velocities render the motion very slow such that the simulation run time becomes impractical for a large Monte Carlo run.

Figure 13 shows the performance comparison result of the simulation. The top panel shows performance results for the scenario size of 24-by-15-by-24-15. The performance curve for the CRN is labeled "adaptive 24-by-24," and the label "rasterized 24-by-24" is for the two-radar platform that uses the rasterized beamsteering strategy. Notice how well the CRN performs compared with the two-radar platform that utilizes the rasterized beamsteering strategy. The bottom panel shows performance results for the scenario size of 30-by-15-by-30-15. The performance curve for the CRN is labeled "adaptive 30-by-30," and the label "rasterized 30-by-30" is for the two-radar platform that uses the rasterized strategy. Again, the CRN performed well compared with the two-radar platform that utilizes the rasterized beamsteering strategy. Note the slight performance degradation due to the larger scenario. A larger scenario means larger coverage time, which may result in performance loss. Notice,

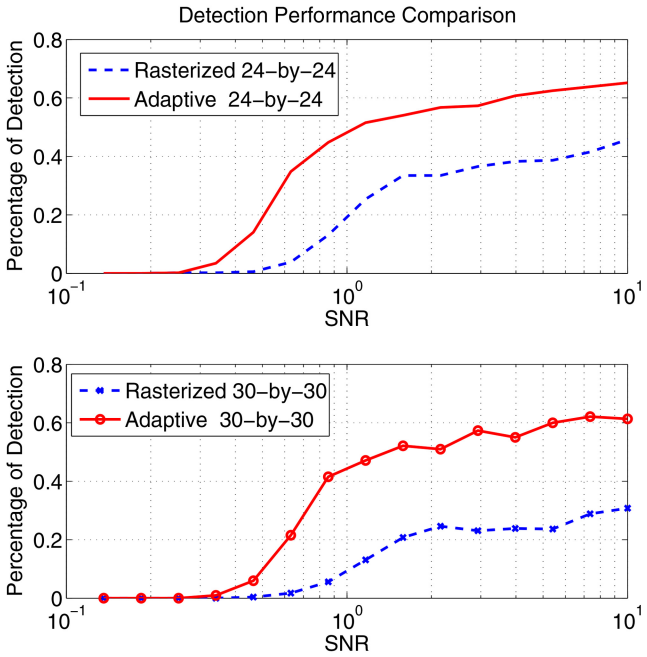

Fig. 13. Performance comparison between two-platform CRN employing adaptive beamsteering strategy and system with two radars employing traditional rasterized beamsteering strategy with search-and-track application in surveillance areas of 24-by-15-by-24-by-15 cells and 30-by-15-by-30-by-15.

however, that the performance degradation for the adaptive 30-by-30 is very small compared with the rasterized 30-by-30, which degraded substantially. This is the effect gained by having a cognizant radar network that dynamically tailors its beamsteering strategy to the channel uncertainties (search and track) as opposed to a system that employs conventional beamsteering.

The limiting detection performance of either systems depends on scenario size, time step size, clutter PSD shape, and other factors. For example, a target may appear and quickly disappear depending on the random draw of its actual positions and velocities. Also, in our simulation, we automatically remove a target once it surpasses the maximum normalized spatial frequency values of -0.5 and 0.5 (edges and corners). This means that, at times, a target may quickly appear, and a particular realization due to target maneuverability may render it to quickly disappear where the CRN or otherwise may not have the time to illuminate that target area. Thus, the fact that detection does not approach 100% is not of particular concern. Instead, in this experiment, we point out the clear advantage of the detection performance of a CRN that employs adaptive beamsteering compared with traditional scanning method.

VII. SUMMARY AND CONCLUSIONS

In this paper we concentrated on the development of a CR system that is geared towards the search-and-track application. This CR system exploits the spatial dimension as a resource via the adaptive beamsteering strategy for the search-and-track application. In designing a matched spatial illumination beamsteering strategy for a two-platform CRN that performs the search-and-track application with four-parameter tracking, we first developed a probabilistic representation or understanding of the channel. This resulted in an ensemble or map of probabilities, where each resolution cell represented a 4-parameter location that any target could occupy. Each cell contained a probability of a target being present. Since each radar could measure only three parameters, we addressed the problem of having ambiguous cells in the dimension that the radar could not measure. We developed a method to update probabilities based on MHT and Bayes' rule. We also developed a dynamic probability model, which reflected the fact that an area could have portions where the likelihood of targets present might be higher than others. Initial estimates of target parameters were needed after detection. For the purposes of simulating our CR system, we used MLE asymptotic properties and used the random-draw method via the CRLB for an initial estimate of our track. We developed a motion model for our moving targets and used a Kalman tracker for tracking detected targets. If tracked targets were not a priority, we developed an adaptive search-only beamsteering strategy to match the search area uncertainty, with BPE as a measure of uncertainty of an area covered by the antenna array's main beamwidth. If tracked targets had some degree of priority, then a strategy was developed such that the target track quality could be maintained while searching for targets. We obtained TTE for a tracked target, the entropy value quantifying the uncertainty of a track. The TTE was a function of the target's SCM. Via a "novel" approach of using a priority dial Ω or scale between the two competing search-and-track needs, a way to compromise between the two priorities was developed. Once a priority value was dictated by a system, the CRN's spatial illumination strategy was matched to the priority needs as quantified by the search-and-track uncertainties, i.e., the resulting adaptive search-and-track beamsteering strategy compromised between searching for targets and tracking detected targets. Various examples with differing scenario sizes were presented. Finally, to show detection performance for our CRN, we compared performance of the CRN with the performance of a two-platform radar system that employed the traditional rasterized beamsteering pattern. In our Monte Carlo simulations, we ensured that both had the same update illumination rate for a tracked target for fair comparison. It was shown that the CRN utilizing the adaptive search-and-track beamsteering strategy outperformed the system that utilized the traditional beamsteering pattern.

APPENDIX. MLE OF TARGET PARAMETERS

Recall, for a single measurement, that the reflection coefficient is constant and that $S(k_x,k_y)$ is fixed such that they can be scaled into $\mathbf{s}(k_x,d_x,k_y)$, where the pdf of the measurement $\mathbf{z}$ with this target signal is

$$p(\mathbf{z};k_x,d_x,k_y) = \frac{1}{\pi^N \det(\mathbf{R})}\exp[-(\mathbf{z}-\mathbf{s}(k_x,d_x,k_y))^H\mathbf{R}^{-1}(\mathbf{z}-\mathbf{s}(k_x,d_x,k_y))]. \tag{37}$$

We desire to find estimates for k_x,d_x,k_y that maximize the above likelihood. It is sometimes convenient to take the $\ln(\cdot)$ of the pdf above such that

$$\ln(p(\mathbf{z};k_x,d_x,k_y)) = \ln\left(\frac{1}{\pi^N \det(\mathbf{R})}\right) - [(\mathbf{z}-\mathbf{s}(k_x,d_x,k_y))^H\mathbf{R}^{-1}(\mathbf{z}-\mathbf{s}(k_x,d_x,k_y))]. \tag{38}$$

Since $\ln(\cdot)$ is a monotonic increasing function, we may maximize the log-likelihood. Moreover, the first term of the right-hand side is a constant and will not affect maximization if ignored. Then, we desire to evaluate

$$\max_{k_x,d_x,k_y} -[(\mathbf{z}-\mathbf{s}(k_x,d_x,k_y))^H\mathbf{R}^{-1}(\mathbf{z}-\mathbf{s}(k_x,d_x,k_y))] \tag{39}$$

which is equivalent to

$$\min_{k_x,d_x,k_y} [(\mathbf{z}-\mathbf{s}(k_x,d_x,k_y))^H\mathbf{R}^{-1}(\mathbf{z}-\mathbf{s}(k_x,d_x,k_y))]. \tag{40}$$

The above expression expands to

$$\min_{k_x,d_x,k_y} [\mathbf{z}^H\mathbf{R}^{-1}\mathbf{z} - \mathbf{z}^H\mathbf{R}^{-1}\mathbf{s}(k_x,d_x,k_y) - \mathbf{s}(k_x,d_x,k_y)^H\mathbf{R}^{-1}\mathbf{z} + \mathbf{s}(k_x,d_x,k_y)^H\mathbf{R}^{-1}\mathbf{s}(k_x,d_x,k_y)]. \tag{41}$$

Notice that the first term does not depend on the target frequencies and that the last term is constant such that the minimization can be evaluated with the middle terms, which simplifies to

$$\min_{k_x,d_x,k_y} [\mathrm{Re}\{\mathbf{z}^H\mathbf{R}^{-1}\mathbf{s}(k_x,d_x,k_y)\}]. \tag{42}$$

REFERENCES

[1] Fuhrmann, D. R.
Active-testing surveillance systems, or, playing twenty questions with a radar.
Proceedings of the 11th Annual Adaptive Sensor and Array Processing (ASAP) Workshop, Lexington, MA, Mar. 11–13, 2003.

[2] Fuhrmann, D. R. and Boggio, L.
Active testing surveillance for multiple target detection with composite hypotheses.
Proceedings of the 2003 IEEE Workshop on Statistical Signal Processing, St. Louis, MO, Sept. 2003, pp. 641–644.

[3] Guerci, J.
Cognitive Radar: The Knowledge-Aided Fully Adaptive Approach.
Norwood, MA: Artech House, 2010.

[4] Haykin, S.
Cognitive radar: A way of the future.
IEEE Signal Processing Magazine, **23**, 1 (Jan. 2006), 30–40.

[5] Goodman, N. A., Venkata, P. R., and Neifeld, M. A.
Adaptive waveform design and sequential hypothesis testing for target recognition with active sensors.
IEEE Journal of Selected Topics in Signal Processing, **1**, 1 (June 2007), 105–113.

[6] Bell, M. R.
Information theory and radar waveform design.
IEEE Transactions on Information Theory, **39**, 5 (Sept. 1993), 1578–1597.

[7] Bell, M. R.
Information theory and radar: Mutual information and the design and analysis of radar waveforms and systems.
Ph.D. dissertation, California Institute of Technology, 1988.

[8] Hyeong-Bae, J. and Goodman, N.
Adaptive waveforms for target class discrimination.
Proceedings of the 2007 Waveform Diversity and Design Conference, Pisa, Italy, June 2007, pp. 395–399.

[9] Romero, R. and Goodman, N.
Improved waveform design for target recognition with multiple transmissions.
Proceedings of the 2009 International Waveform Diversity and Design Conference, Kissimmee, FL, Feb. 8–13, 2009, pp. 26–30.

[10] Romero, R. and Goodman, N.
Waveform design in signal-dependent interference and application to target recognition with multiple transmissions.
IET Radar, Sonar and Navigation, **3**, 4 (Aug. 2009), 328–340.

[11] Chen, Y. and Rapajic, P.
Ultra-wideband cognitive interrogator network: Adaptive illumination with active sensors for target localization.
IET Communications, **5**, 4 (Oct. 2008), 325–333.

[12] Nielsen, P.
Adaptive spatial-domain beam steering in a wide area search and track application.
Master's thesis, University of Arizona, 2009.

[13] Romero, R. and Goodman, N.
Adaptive beamsteering for search-and-track application with cognitive radar network.
Proceedings of the 2011 IEEE Radar Conference (RADAR), Kansas City, MO, May 23–27, 2011, pp. 1091–1095.

[14] Levanon, N.
Radar Principles.
Hoboken, NJ: Wiley, 1988.

[15] Romero, R. and Goodman, N.
Channel probability ensemble update for multiplatform radar systems.
Proceedings of the 2010 International Waveform Diversity and Design Conference, Niagara Falls, Canada, Aug. 8–13, 2010, pp. 182–187.

[16] Cover, T. M. and Thomas, J. A.
Elements of Information Theory.
Hoboken, NJ: Wiley, 1991.

[17] Peebles, P.
Radar Principles.
Hoboken, NJ: Wiley, 1998.

[18] Shannon, C.
A mathematical theory of communications.
Bell System Technical Journal, **27** (July 1948), 379–423.

[19] Fuhrmann, D. R.
One-step optimal measurement selection for linear Gaussian estimation problems.
Proceedings of the 2007 Waveform Diversity and Design Conference, Pisa, Italy, June 4–8, 2007, pp. 224–227.

[20] Kay, S.
Fundamentals of Statistical Signal Processing, vol. I, Estimation Theory.
Upper Saddle River, NJ: Prentice-Hall, 1993.

[21] Van Trees, H.
Optimum Array Processing.
Hoboken, NJ: Wiley, 2002.

[22] Romero, R. A.
Matched waveform design and adaptive beamsteering in cognitive radar applications.
Ph.D. dissertation, University of Arizona, 2010.

[23] Fuhrmann, D. R. and Antonio, G. S.
Kalman filter and extended Kalman filter using one-step optimal measurement selection.
Proceedings of the 2007 Waveform Diversity and Design Conference, Pisa, Italy, June 4–8, 2007, pp. 312–315.

Ric A. Romero (S'07—M'10—SM'12) received his Ph.D in electrical and computer engineering from the University of Arizona in 2010, his MSEE degree from the University of Southern California in 2004, and his BSEE from Purdue University in 1999.

From 1999–2010 he was a Senior Multidisciplined Engineer II at Raytheon Missile Systems in Tucson, Arizona. He was involved in various communications, radar, and research and development programs. He was also a graduate research assistant at the Laboratory for Sensor and Array Processing, University of Arizona, from 2007–2010. He is currently an assistant professor in the Department of Electrical and Computer Engineering, Naval Postgraduate School, Monterey, CA. His research interests are in the general areas of radar, sensor information processing, and communications.

Dr. Romero was awarded the 2004 Corporate Excellence in Technology Award, a company-wide technical prize at Raytheon Corporation. He was also granted the Raytheon Advanced Scholarship Program fellowships from 2002–2004 and 2005–2007.

Nathan A. Goodman (S'98—M'02—SM'07) received his B.S., M.S., and Ph.D. degrees in electrical engineering from the University of Kansas, Lawrence, in 1995, 1997, and 2002, respectively.

From 1996 to 1998 he was an RF systems engineer for Texas Instruments, Dallas, TX. From 1998 to 2002 he was a graduate research assistant in the Radar Systems and Remote Sensing Laboratory, University of Kansas. He was a faculty member in the Department of of ECE at the University of Arizona, Tucson, from 2002 to 2011, and he is now an associate professor in the School of Electrical and Computer Engineering at the University of Oklahoma, Norman. His research interests are in radar and array signal processing.

Dr. Goodman was awarded the Madison A. and Lila Self Graduate Fellowship from the University of Kansas in 1998. He also received the IEEE 2001 International Geoscience and Remote Sensing Symposium Interactive Session Prize Paper Award. He has served as the technical cochair for the 2011 IEEE Radar Conference, the finance chair for the 2012 SAM workshop, and the associate editor-in-chief for Elsevier's *Digital Signal Processing* journal. He is currently an associate editor for *IEEE Transactions on Aerospace and Electronic Systems*.